Bulky pyrazolate-based compartmental ligand scaffolds: encapsulation of an edge-sharing Cu_6O_2 bitetrahedral core

Anna Sachse,[a] Gilles Noël,[a] Sebastian Dechert,[a] Serhiy Demeshko,[a] Andreas Honecker,[b] Alexei Alfonsov,[c] Vladislav Kataev[c] and Franc Meyer*[a]

[a] Institut für Anorganische Chemie, Georg-August-Universität Göttingen
Tammannstrasse 4, D-37077 Göttingen, Germany
Fax: +49 551 / 393063
E-mail: franc.meyer@chemie.uni-goettingen.de

[b] Institut für Theoretische Physik, Georg-August-Universität Göttingen
Friedrich-Hund-Platz 1, D-37077 Göttingen, Germany

[c] Institute for Solid State Physics IFW Dresden
Helmholtzstrasse 20, D-01069 Dresden, Germany

Received

Keywords: Oligonuclear complexes / N ligands / copper / μ_4-oxo ligands / magnetic properties

Upon reaction with $Cu(OAc)_2 \cdot H_2O$, pyrazole-based ligands with two appended imine chelate arms in the 3- and 5-positions of the pyrazole and bulky substituents at the imine-N yield Cu_6-complexes $[L_2Cu_6(\mu\text{-}OAc)_6(\mu_4\text{-}O)_2]$ (**1a**,**b**). They feature an unusual $\{Cu_6(\mu_4\text{-}O)_2\}$-bitetrahedral core, the only second example for this structural motif. ESI mass spectrometric and UV/vis data confirm that the Cu_6-complexes stay intact in solution, and magnetic and high-field EPR measurements reveal an $S = 0$ ground state with the first excited triplet at $\Delta E \approx 95$ cm^{-1}. Although the new hexanuclear systems are too complex for deriving all individual exchange constants from powder susceptibility data, a rough idea of the complete energy level spectrum could be obtained.

Supporting Information for this article is available on the WWW under http://asc.wiley-vch.de/home/

Dedicated to Prof. Dr. Jan Reedijk on the occasion of his retirement

Introduction

Pyrazolate-based ligands with chelating side arms in the 3- and 5-positions of the diazole heterocycle have been established as valuable compartmental scaffolds for the targeted construction of bi- and oligonuclear transition metal complexes.[1,2] Incorporation of metal ions in the two proximate binding sites may lead to cooperative effects in electronic or magnetic properties as well as in metal-mediated transformations of substrate molecules.[3,4,5,6] In this context we have recently prepared a series of novel pyrazole-diimine ligands L with bulky aryl substituents at the imine-N and variable backbone substituents R, together with their nickel(II) and palladium(II) complexes (e.g., **A**).[7,8,9] Those complexes can be viewed as bimetallic versions of the prominent α-diimine derived Brookhart-type precatalysts for olefin polymerization, and indeed some pyrazolate-based bimetallic systems have been shown to exhibit high activity in the polymerization of ethylene.[8] In the case of nickel and if aryl substituents are not too bulky, however, species $\{LNi_2X_3\}$ with X = Cl, Br) tend to aggregate to give tetra- or hexanuclear complexes such as $[LNi_2X_3]_3$ with unusual nickel-halide structural motifs.[7,9] This suggests to use such pyrazole-diimine ligands for the wrapping and stabilisation of other metal clusters. In pursuit of further exploring the coordination properties of the pyrazole-diimine ligand system, we here report two copper(II) complexes that feature a central edge-sharing Cu_6O_2 bitetrahedral core encapsulated by two ligand scaffolds L, and their magnetic properties.

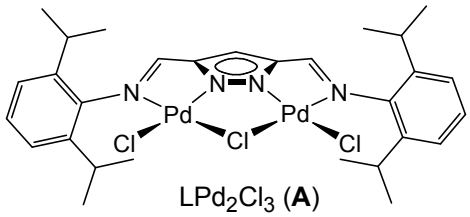

LPd_2Cl_3 (**A**)

Results and Discussion

Synthesis and structural characterization

Dinucleating ligands HL^1 and HL^2 can be synthesized in five steps from commercially available material as reported.[10,8] Complex $[L^1{}_2Cu_6(\mu\text{-}OAc)_6(\mu_4\text{-}O)_2]$ (**1a**) was initially obtained in low yields from a reaction mixture containing HL^1, one equivalent of KO*t*Bu (to deprotonate the pyrazole) and two equivalents of $Cu(OAc)_2{\cdot}H_2O$, which was anticipated to give a dicopper(II) species of type $LCu_2(OAc)_3$. Once the identity of **1a** was established,

however, it could be prepared in much better yields up to 87% by simply adding three equivalents of the copper salt to a solution of HL^1 in THF (Scheme 1). In the latter reaction the acetate also serves as a base for deprotonation of the pyrazole ligand and of water. The corresponding complex $[L^2{}_2Cu_6(\mu\text{-}OAc)_6(\mu_4\text{-}O)_2]$ (**1b**) was obtained under identical conditions when starting from HL^2. Both complexes have been fully characterized by elemental analysis, mass spectrometry, IR and UV/Vis spectroscopy, and X-ray crystallography (see Experimental Section for details), as well as by magnetic measurements (for **1a**). The molecular structure of **1a** established from the X-ray data is depicted in Fig. 1. The molecular structure of **1b** is basically identical and is shown in Figure S1. Selected atom distances and bond angles for both complexes are listed in Table 1.

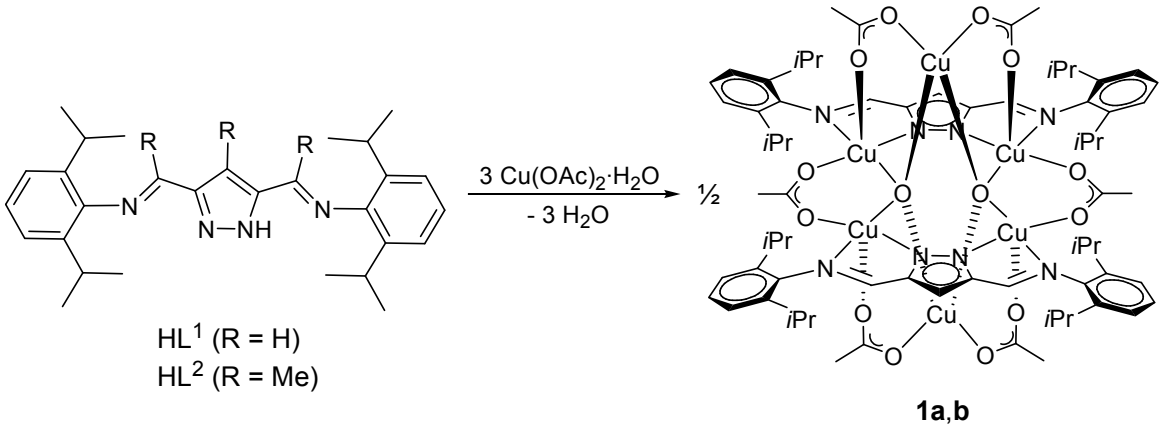

Scheme 1. Synthesis of **1a**,**b**; for the sake of clarity substituents R have been omitted in the products

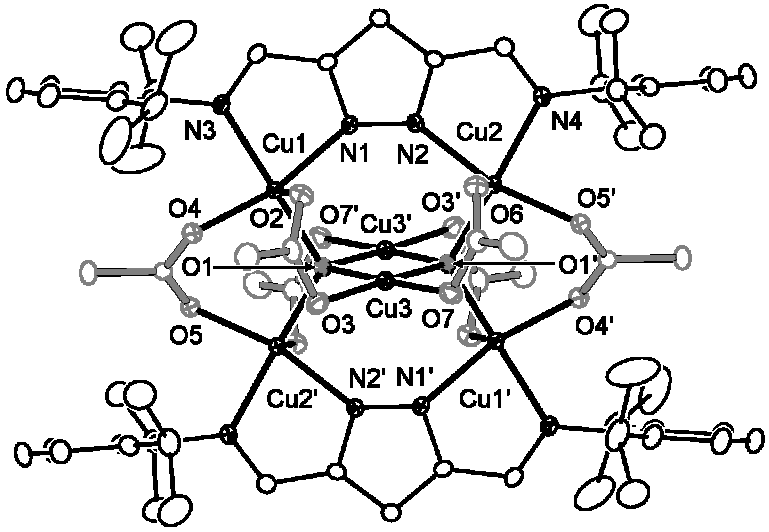

Figure 1. ORTEP plot (30% probability thermal ellipsoids) of the molecular structure of **1a**. For the sake of clarity all hydrogen atoms have been omitted. Symmetry transformation used to generate equivalent atoms: (') 1-*x*, 1-*y*, 1-*z*.

Table 1. Selected atom distances [Å] and bond angles [°] for **1a** and **1b**.*

	1a	**1b**
Cu1-O1	1.9103(19)	1.912(4)
Cu2-O1'	1.9148(19)	1.923(4)
Cu3-O1	1.9342(19)	1.933(3)
Cu3-O1'	1.9288(18)	1.939(3)
Cu1-O2	2.258(2)	2.239(4)
Cu1-N1	2.042(2)	2.055(4)
Cu1-N3	2.062(2)	2.048(4)
Cu2-O6	2.224(2)	2.229(4)
Cu2-N2	2.049(2)	2.042(4)
Cu2-N4	2.062(2)	2.052(4)
Cu3-O3	1.956(2)	1.951(4)
Cu3-O7	1.947(2)	1.957(4)
Cu(1)···Cu(2)	4.4446(4)	4.4247(8)
Cu(1)···Cu(2')	3.3185(4)	3.3378(9)
Cu(1)···Cu(3)	3.0501(5)	3.0576(9)
Cu(2)···Cu(3)	3.0962(5)	3.0822(9)
Cu(1)···Cu(3')	3.1866(5)	3.2006(8)
Cu(2)···Cu(3')	3.1908(5)	3.1930(8)
Cu(3)···Cu(3')	2.9083(7)	2.9273(12)
O(1)···O(1')	2.5426(27)	2.5358(43)
O(1)-Cu(1)-O(4)	97.44(8)	97.10(15)
O(1)-Cu(1)-N(1)	96.44(8)	97.45(15)
O(1)-Cu(1)-N(3)	159.28(9)	159.00(16)
O(1')-Cu(3)-O(1)	82.32(8)	81.80(13)
N(1)-Cu(1)-N(3)	80.23(9)	79.54(16)
O(1')-Cu(2)-N(2)	95.69(8)	97.30(16)
O(1')-Cu(2)-N(4)	160.00(9)	159.18(16)
N(2)-Cu(2)-N(4)	79.91(9)	80.12(16)
Cu(1)-O(1)-Cu(2')	120.35(9)	120.98(15)
Cu(1)-O(1)-Cu(3')	112.20(9)	112.65(19)
Cu(2')-O(1)-Cu(3')	107.32(9)	106.11(16)
Cu(1)-O(1)-Cu(3)	105.00(9)	105.08(16)
Cu(2')-O(1)-Cu(3)	111.99(9)	111.51(19)
Cu(3')-O(1)-Cu(3)	97.68(8)	98.20(13)
N(2)-N(1)-Cu(1)	139.45(18)	139.3(4)
N(1)-N(2)-Cu(2)	139.41(18)	139.9(4)

* Symmetry transformation used to generate equivalent atoms: (') 1-*x*, 1-*y*, 1-*z*.

The C_i-symmetric complexes contain six metal atoms of which two crystallographically independent copper atoms are bridged by the pyrazolate ligand. Two of these pyrazolate-based {LCu_2} building blocks are linked via two acetate bridges, and the resulting rectangle of four copper ions clasps around two further copper ions (Cu3 and Cu3'). The central arrangement of six copper ions constitutes two oxygen-centred edge-sharing tetrahedra, where six of the other edges are spanned by acetate bridges. In crystallopgraphic view there is a {$LCu_3(\mu\text{-}OAc)_3$} unit connected via μ_4-oxo bridges with its symmetry related counterpart.

The coordination environment for the pyrazolate-bound copper atoms in **1a**,**b** is distorted square pyramidal with a distinctly elongated apical Cu-$O_{acetate}$ bond. The third copper is exclusively coordinated by oxygen atoms, giving a distorted square planar coordination sphere. Cu-O distances of the edge-sharing bitetrahedral core with the two μ_4-oxo atoms range from 1.91 to 1.93 Å (Figure 2). Due to the different binding sites of the metal atoms the Cu···Cu distances vary from 2.91 Å for the doubly oxo-briged Cu(3)···Cu(3') located on the shared edge to 3.34 Å for the pyrazolate-bound acetato/oxo-briged atoms Cu(1) and Cu(2') at the external vertices of the bitetrahedron, resulting in Cu-O-Cu angles that are quite far from being perfectly tetrahedral. The angles span the range from 97.7° for Cu(3)-O(1)-Cu(3') to 121.0° for Cu(1)-O(1)-Cu(2'). Cu-O-Cu angles are considered important for the magnetic coupling between copper(II) ions bridged by ligand O atoms (oxo, hydroxo, alkoxo, etc.), which is discussed in more detail below.

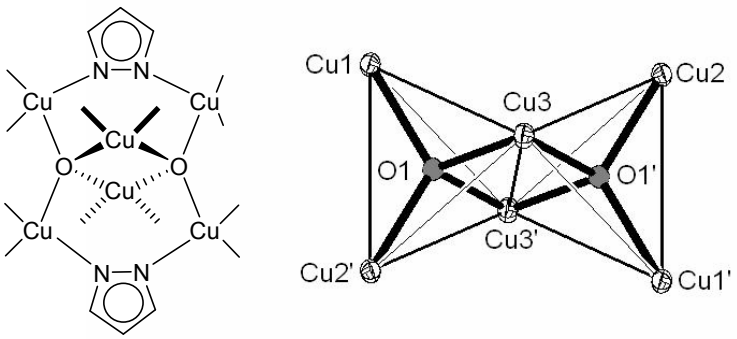

Figure 2. Emphasis of the {$Cu_6(\mu_4\text{-}O)_2$}-bitetrahedron in **1a**. Symmetry transformation used to generate equivalent atoms: (') 1-*x*, 1-*y*, 1-*z*.

While tetranuclear complexes with a $\{Cu_4(\mu_4\text{-}O)\}$ kernel are quite abundant and well studied,[11,12,13,14] only one previous example for the present structural motive of a $\{Cu_6(\mu_4\text{-}O)_2\}$-bitetrahedron has been reported, namely for octanuclear copper(II) acetate complexes with pyridonate ligands of the general formula $[Cu_8(O_2)(O_2CCH_3)_4L_8]$ (L = 6-chloro, 6-bromo, 6-methyl-2-pyrodinate).[15] Interestingly, in those cases the $\{Cu_6(\mu_4\text{-}O)_2\}$ core is distorted in the same manner as in **1a**,**b**, despite significant differences in the ligand type and the overall constitution of the complexes. The shortest Cu···Cu distances and the smallest Cu-O-Cu angles in the pyridonate complexes were observed for the copper-atoms located on the shared edge (2.92 to 2.95 Å and 95 to 98°), the longest Cu···Cu distances and widest Cu-O-Cu angles for the copper atoms located on the external vertices (3.48 to 3.58 Å and 136 ± 4°). Since there is no additional bridge between the external edges $[Cu_8(O_2)(O_2CCH_3)_4L_8]$, the latter distances are 0.2 to 0.3 Å longer than in **1a**,**b**.

UV/Vis spectra at room temperature in CH_2Cl_2 solution (Figures 3 and S2) show a series of intense ligand π-π^* and LMCT absorptions below 370 nm, and a weak broad band at 740 nm (**1a**) or 748 nm (**1b**) that is assigned to d-d transitions of the copper(II) ions. Since the same UV/Vis spectral features are observed when **1a**,**b** are measured as solids in diffuse reflectance mode, it can be assumed that the hexanuclear entities found in the solid state structures are also stable in solution.

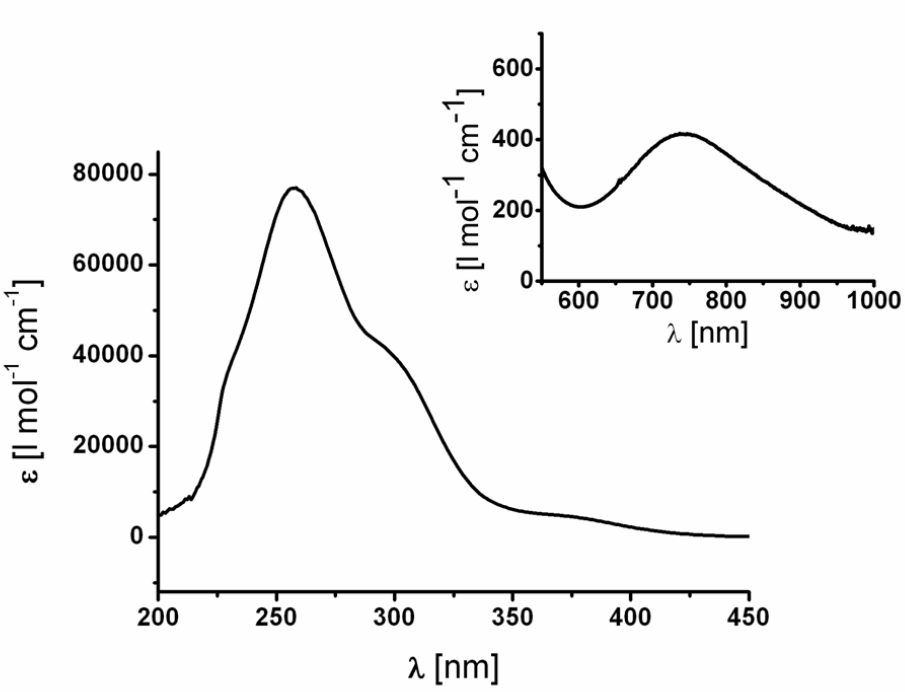

Figure 3. UV/Vis spectrum for **1a** in CH_2Cl_2 solution; The inset shows an enlargement of the d-d transition band for the Cu^{II} ions with λ_{max} = 740 nm (ε = 416 l·mol^{-1}·cm^{-1}).

This is further corroborated by ESI mass spectrometry of solutions of the complexes in MeCN / CH_2Cl_2, which show prominent peaks for the ions $[L_2Cu_6O_2(OAc)_5]^+$, *e.g.*, for the molecular ions devoid of a single acetate (Figures 4 and S3).

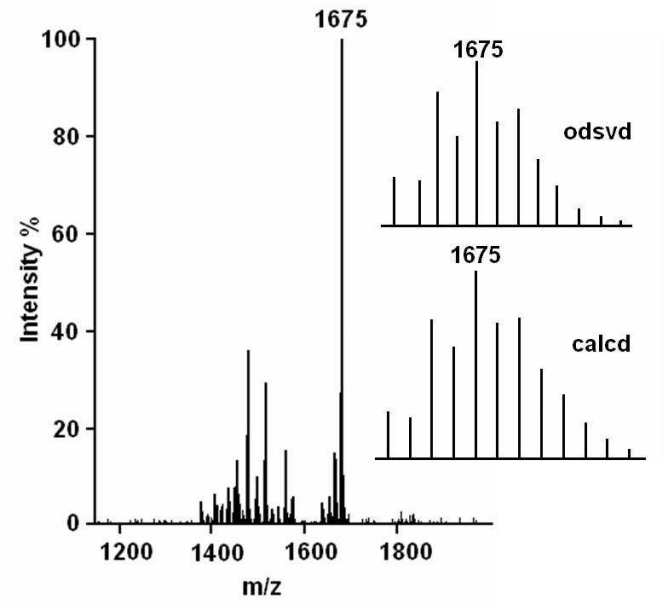

Figure 4. Positive ion ESI-MS spectrum for **1b** in MeCN / CH_2Cl_2 solution; the inset shows the experimental and calculated isotopic distribution for the peak at *m*/*z* 1675 corresponding to $[L^2{}_2Cu_6O_2(OAc)_5]^+$.

Magnetic and EPR properties

Magnetic susceptibility data were collected for **1a** in the temperature range from 295 to 2.0 K in order to characterize the exchange coupling within the hexanuclear copper(II) core. No significant field dependence was observed when data were measured at applied fields of 0.2 and 0.5 T. The temperature dependence of the molar magnetic susceptibility χ_M and of the product $\chi_M T$ are shown in Figure 5. The observed $\chi_M T$ value at room temperature is 2.21 $cm^3 \cdot K \cdot mol^{-1}$ (corresponding to an effective moment $\mu_{eff} = 4.21\ \mu_B$), slightly smaller than the theoretical value expected for six uncoupled copper(II) ions (2.53 $cm^3 \cdot K \cdot mol^{-1}$ or $\mu_{eff} = 4.50\ \mu_B$ for $g = 2.12$). Upon lowering the temperature, χ_M goes through a broad maximum at around 130 K and $\chi_M T$ gradually tends to zero, in accordance with overall antiferromagnetic coupling and an $S = 0$ ground state. The rise of χ_M at very low temperatures is assigned to the Curie tail caused by minor amounts of paramagnetic impurities (presumably mononuclear Cu^{II} species).

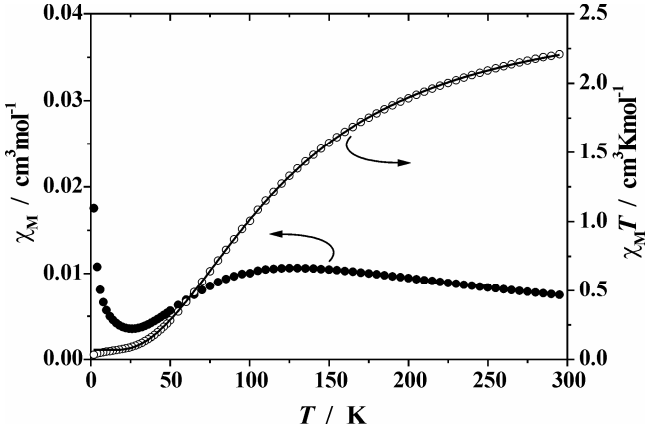

Figure 5. Plot of χ_M (solid circles) and $\chi_M T$ (open circles) vs. T for **1a** at 0.5 T; the solid line represents the calculated curve fit (see text).

For both complexes, EPR has been studied at a constant microwave frequency of 93 GHz in magnetic fields up to 6 T with the experimental setup described in ref.[4] A weak and broad absorption peak could only be detected at temperatures around 120 - 130 K (see Figure S4), i.e. in the temperature range where χ_M values are highest. The peak maximum occurs at a resonance field of ~3.13 T which corresponds to a *g*-factor of 2.12. The EPR signal can be assigned to overlapping resonance transitions obeying the EPR selection rule $\Delta S^z = \pm 1$ within the thermally populated excited states multipletts (S = 1, etc.). Though the maximum gain of the spectrometer was used, no weak quasi-forbidden transitions $\Delta S^z = \pm 2$ at a half resonance field have been observed.[16] The somewhat asymmetric signal line shape of the powder spectrum may indicate *g*-factor anisotropy, which is common for Cu^{2+}.[17] The above estimate g = 2.12 should therefore be considered as a mean *g* value.

Magnetic properties have been analyzed in terms of a Heisenberg model according to eq. (1)

$$\begin{aligned} H = &-2J_1\vec{S}_3\cdot\vec{S}_4 + J_2\left(\vec{S}_1\cdot\vec{S}_2+\vec{S}_5\cdot\vec{S}_6\right) - 2J_3\left(\vec{S}_1\cdot\vec{S}_5+\vec{S}_2\cdot\vec{S}_6\right) \\ &-2J_4\left(\vec{S}_4\cdot\left(\vec{S}_1+\vec{S}_5\right)+\vec{S}_3\cdot\left(\vec{S}_2+\vec{S}_6\right)\right) \\ &-2J_5\left(\vec{S}_3\cdot\left(\vec{S}_1+\vec{S}_5\right)+\vec{S}_4\cdot\left(\vec{S}_2+\vec{S}_6\right)\right) \end{aligned} \qquad (1)$$

which corresponds to the coupling scheme sketched in Figure 6. Here, the $\vec{S}_i$ are spin –1/2 operators. Note that we use conventions such that $J_i < 0$ corresponds to antiferromagnetic exchange. In comparison with ref. 15, which uses a similar model for the only other $\{Cu_6(\mu_4\text{-}O)_2\}$-bitetrahedron reported to date, we allow for one additional exchange path J_3 and a larger number of independent exchange constants.

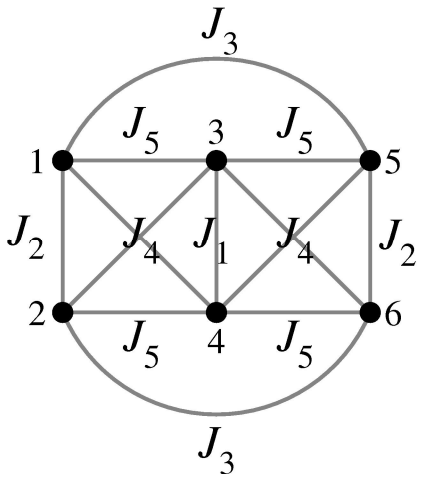

Figure 6. Magnetic coupling scheme for the six copper(II) ions in the bitetrahedral core. Dots correspond to the copper ions of Figure 2.

Once all $2^6 = 64$ eigenvalues E_i of the Hamiltonian (1) and the corresponding quantum numbers S_i^z of the *z*-component of the total spin of a molecule are obtained, the magnetic susceptibility can be computed according to eq. (2)

$$\chi_0 = \frac{N_A g^2 \mu_B^2}{k_B T} \frac{\sum_i \left(S_i^z\right)^2 e^{-E_i / k_B T}}{\sum_i e^{-E_i / k_B T}}, \tag{2}$$

where N_A is Avogadro's constant, μ_B is the Bohr magneton, and k_B is Boltzmann's constant. In addition, an impurity contribution given by the susceptibility of free spins with S = ½ is included (eq. (3)).

$$\chi_{\text{Imp.}} = \frac{N_A g^2 \mu_B^2}{4 k_B T}. \tag{3}$$

Taking g = 2.12 from the EPR analysis, six parameters remain in the total magnetic susceptibility $\chi_M = \chi_0 + C\chi_{\text{Imp.}}$. In order to further reduce the number of free parameters to not more than five, we assume that $J_5 = J_4$, which in view of the similarity of the underlying exchange paths should be a reasonable approximation: both J_4 and J_5 represent couplings between a square-planar and a square-pyramidal copper(II) linked by a μ_4-O, the only difference being the additional acetate bridge in one of the two paths. It is fair to assume that magnetic coupling is mainly determined by the μ_4-O linkage, even more so since the acetate displays only a weak Jahn-Teller elongated bond to the apical position of the square-pyramidal copper(II), while the magnetic orbital is the basal $d_{x^2-y^2}$. The assumption $J_5 = J_4$ has several side effects. Firstly, it renders J_2 and J_3 equivalent by symmetry (see Figure 6), so that J_2 and J_3 are not unambiguously assigned to topological J values. Accordingly, fits to

macroscopic properties will come in pairs which differ by an interchange of J_2 and J_3. Secondly, with $J_5 = J_4$ it is now possible to obtain the eigenvalues in closed form, although the explicit expressions are too cumbersome to be presented here. Such an analytic solution is useful for fitting purposes.

A least-squares fit of the model (1) to the experimental magnetic susceptibility shown in Figure 5 has been performed, yielding parameters sets (a) - (d) for four equally good and physically reasonable fits (Table 2). Note firstly that the interchange of values of J_2 and J_3 gives another equivalent fit for each parameter set. Secondly, note that a pure dimer fit, i.e., a fit with $J_3 = J_4 = J_5 = 0$ yields obviously worse agreement with experiment.

Table 2. Exchange constants determined from fits to the magnetic susceptibility, in Kelvin and cm^{-1} (in brackets).

	(a)	(b)	(c)	(d)
J_1	–68.5 (–47.6)	–125.4 (–87.2)	–164.8 (–114.5)	–69.7 (–48.4)
J_2	–161.9 (–112.5)	–100.8 (–70.1)	–78.4 (–54.5)	–135.7 (–94.3)
J_3	–59.7 (–41.5)	151.4 (105.2)	–50.6 (–35.2)	59.0 (41.0)
$J_5 = J_4$	52.9 (36.7)	–6.2 (–4.3)	39.1 (27.2)	12.5 (8.7)
C	0.1612	0.1604	0.1610	0.1627

The line shown in Figure 5 represents the parameter set (a), but it should be noted that all four parameter sets result in fits of comparable quality for the magnetic susceptibility and are indistinguishable on the scale of Figure 5. In fact, it can be seen from Table S1 that all four parameter sets listed in Table 2 lead to very similar eigenvalue spectra. However, parameter set (a) appears to be most reasonable when considering known magnetostructural correlations: (i) strongest antiferromagnetic coupling (J_2 = –112.5 cm^{-1}) occurs for the (μ_4-oxo)(μ-carboxylato)-bridged pairs of copper ions (Cu1···Cu2'), as the angle Cu1-O1-Cu2' is very large (120.35(9)°) and the bridges lie within the plane of the copper magnetic orbitals. (ii) Relatively weak or moderate antiferromagnetic coupling is common for singly pyrazolato-bridged copper(II) ions (Cu1···Cu2; J_3 = –41.5 cm^{-1}).[18] (iii) Magnetic orbitals of the square-planar Cu3 and square-pyramidal Cu1/Cu2 are mutually orthogonal, and hence the coupling is ferromagnetic ($J_5 = J_4$ = +36.7 cm^{-1}).[19] (iv) For the copper(II) ions located at the shared edge of the {$Cu_6(\mu_4\text{-}O)_2$}-bitetrahedron one might have expected a very weakly antiferromagnetic or even ferromagnetic coupling because of the small bridging angle Cu3-O1'-Cu3' of 97.68(8)°,[19,20] but all parameter sets that represent good quality fits reveal significant antiferromagnetic coupling, e.g., J_1 = –47.6 cm^{-1} for set (a). In contrast to this, but in line with expectations, ferromagnetic coupling has been observed in a hexanuclear copper(II) cluster

(with topology very different from that of **1a**,**b**) that contains a central Cu(μ-OH)$_2$)Cu link and Cu-O(H)-Cu angles of 95.1°.[21] One may conclude that the correlation between J and bridging angle established for Cu(μ-OH)$_2$Cu cores[20] does not necessarily hold for the Cu(μ$_4$-O)Cu motif.

Although one cannot unambiguously determine the exchange constants J_i uniquely from the susceptibility alone, we have the following robust features: (i) the ground state of the molecule is a singlet (total spin $S = 0$); (ii) the first excited stated is a triplet ($S = 1$) with an excitation energy $\Delta E \approx 140$ K (≈ 95 cm^{-1}); (iii) the state with maximal spin $S = 3$ is located at $\Delta E \approx 600$ K (≈ 400 cm^{-1}); (iv) the complete spectrum is spread over an energy range $\Delta E \approx 1000$ K (≈ 700 cm^{-1}) (compare Table S1); and (v) the sample has an impurity contribution corresponding to $C/6 \approx 2.7\%$ of the atoms (see Table 2). Since the different parameter sets (a) – (d) yield very similar physical properties, it will be impossible to single one of them out by thermodynamic or even spectroscopic measurements. Rather, one would need additional microscopic information, e.g., on the local spin arrangement in the ground state in order to further narrow down the possible parameter sets without using information on the quantum chemical origin of the exchange processes.

Conclusion

Following their use in nickel and palladium chemistry, pyrazole ligands with appended imine chelate arms have now proven valuable for stabilizing larger metal aggregates also for copper(II), shown here for the novel Cu$_6$-complexes **1a**,**b** that feature an unusual {Cu$_6$(μ$_4$-O)$_2$}-bitetrahedral core, the only second example for this structural motif. Spectroscopic and other data confirm that the Cu$_6$-complexes stay intact in solution, and magnetic and high-field EPR data reveal an $S = 0$ ground state with the first excited triplet at $\Delta E \approx 95$ cm^{-1}. Although the new hexanuclear systems are too complex for deriving all individual exchange constants from powder susceptibility data, a rough idea of the complete energy level spectrum could be obtained.

Experimental Section

General

HL^1 and HL^2 were synthesized according to the published procedures,[10,8] Cu(OAc)$_2$·H$_2$O was purchased from Aldrich and used as received. Mass spectra were recorded with a Finnigan MAT 95 (FAB) and a Finnigan LCQ (ESI), IR spectra from KBr peletts with a Digilab Excalibur Series FTS 3000 spectrometer and UV/Vis spectra with an Analytik Jena

Specord S100 or a Varian Cary 5000 spectrometer. Elemental analyses were measured by the analytical laboratory of the Institut für Anorganische Chemie der Universität Göttingen using a Heraeus CHN-O-RAPID instrument. Susceptibility measurements were carried out with a Quantum-Design MPMS-5S SQUID magnetometer equipped with a 5 Tesla magnet in the range from 295 to 2.0 K (**1a**) or 400 to 2.0 K (**1b**). The powdered samples were contained in a gel bucket and fixed in a non-magnetic sample holder. Each raw data file for the measured magnetic moment was corrected for the diamagnetic contribution of the sample holder and the gel bucket. The molar susceptibility data were corrected using the Pascal constant and the increment method. EPR spectra have been collected with a home-made high-field EPR spectrometer on the basis of the Millimeterwave Vector Network Analyzer from AB Millimetre, Paris, and a 15 T superconducting magnet from Oxford Instruments Inc. For EPR measurements the powder material was pressed into a pellet and put in the probehead operating in the transmission mode. The amplitude and the phase of the microwave radiation of a constant frequency transmitted through the pellet have been recorded as a function of the magnetic field strength. The sample temperature in the range 2 – 300 K was regulated by a built-in He-gas flow variable temperature inset.

$[L^1_2Cu_6(\mu_4\text{-}O)_2(\mu\text{-}OAc)_6]$ (1a): To a stirred solution of HL^1 (220 mg, 0.5 mmol) in THF (50 ml) was added $Cu(OAc)_2 \cdot H_2O$ (300 mg, 1.5 mmol). The resulting suspension was stirred for 24 h at room temperature and then evaporated to dryness. Brown crystals of the product **1a** gradually formed by recrystallisation from CH_2Cl_2 or THF solutions. Yield: 360 mg (87%). IR (KBr) (cm^{-1}): 3446 br, 3065 w, 2964 m, 2926 w, 2869 w, 2359 w, 2336 w, 2077 br, 1622 vs, 1586 vs, 1437 s, 1405 m, 1352 w, 1341 w, 1308 w, 1258 w, 1182 w, 1131 w, 1105 w, 1036 w, 933 w, 899 w, 801 w, 743 w, 675 w, 617 w, 578 w, 420 w. UV/Vis (CH_2Cl_2) λ [nm] (ε [L $mol^{-1}cm^{-1}$]): 231 (38450), 257 (76880), 300 (39540), 374 (4597), 740 (416). UV/Vis (diffuse reflectance, KBr) λ [nm]: 219, 254, 381, 469, 730. FAB-MS (nibeol) *m/z* (%): 1577 (11) $[L_2Cu_6(\mu_4\text{-}O)_2(\mu\text{-}OAc)_4 - H + 2Na]^+$, 1514 (3) $[L_2Cu_5(\mu_4\text{-}O)_2(\mu\text{-}OAc)_4 + 2Na]^+$, 1162 (15) $[L_2Cu_4 + Na]^+$, 1073 (100) $[L_2Cu_3]^+$, 1010 (24) $[L_2Cu_2 + H]^+$. ESI-MS (CH_3CN/CH_2Cl_2) *m/z* (%): 1591 (48) $[L_2Cu_6(\mu_4\text{-}O)_2(\mu\text{-}OAc)_5]^+$. Elemental analysis (%): calcd. for $C_{70}H_{92}Cu_6N_8O_{14} \cdot CH_2Cl_2$ (1735.7): C 49.12 H 5.46 N 6.46; found: C 49.03, H 5.85, N 6.82;

$[L^2_2Cu_6(\mu_4\text{-}O)_2(\mu\text{-}OAc)_6]$ (1b): This complex was prepared analogous to **1a**, but starting from HL^2. Green-brown crystals of the product **1b** gradually formed by recrystallisation from CH_2Cl_2 or THF solutions. Yield: 147 mg (41%). IR (KBr) (cm^{-1}): 3428 br, 3063 w, 2965 m,

2929 w, 2869 w, 2360 w, 2339 w, 2066 w, 1603 vs, 1586 vs, 1500 w, 1433 s, 1364 w, 1329 m, 1255 w, 1234 w, 1188 w, 1102 w, 1058 w, 1019 w, 967 w, 935 w, 852 w, 802 w, 774 m, 729 w, 676 w, 619 w, 577 w, 530 w, 456 w. UV/Vis (CH_2Cl_2) λ [nm] (ε [L $mol^{-1}cm^{-1}$]): 229 (61330), 258 (124020), 303 (50550), 368 (8324), 748 (405). UV/Vis (diffuse reflectance, KBr) λ [nm]: 221, 262, 370, 474, 733. FAB-MS (nibeol) *m/z* (%): 1246 (11) $[L_2Cu_4 + Na]^+$, 1157 (22) $[L_2Cu_3]^+$, 609 (38) $[LCu_2]^+$. ESI-MS (CH_3CN/CH_2Cl_2) *m/z* (%): 1675 (100) $[L_2Cu_6(\mu_4\text{-}O)_2(\mu\text{-}OAc)_5]^+$. Elemental analysis (%): calcd. for $C_{76}H_{104}Cu_6N_8O_{14}\cdot 2CH_2Cl_2$ (1904.8): C 49.18, H 5.71, N 5.88; found: C 49.17, H 5.98, N 5.94.

X-ray crystallography: X-ray data were collected on a STOE IPDS II diffractometer (graphite monochromated Mo-Kα radiation, λ = 0.71073 Å) by use of ω scans at –140 °C. The structures were solved by direct methods and refined on F^2 using all reflections with SHELX-97.[22] The non-hydrogen atoms were refined anisotropically. Hydrogen atoms were placed in calculated positions and assigned to an isotropic displacement parameter of 0.08 $Å^2$ (**1a**) or were set at 1.5 U_{eq}(C) for methyl H atoms and 1.2 U_{eq}(C) for other C-bound H atoms (**1b**). Face-indexed absorption corrections were performed numerically with the program X-RED.[23] One CH_2Cl_2 in **1a** is disordered about a crystallographic centre of inversion and was refined with a fixed occupancy factor of 0.5. Two DFIX restraints ($d_{C\text{-}Cl}$ = 1.75 Å) were applied to model the disorder. In **1b** three THF are disordered about two positions and were refined using SAME restraints.

CCDC 687795 (**1a**) and 687796 (**1b**) contain the supplementary crystallographic data for this paper. These data can be obtained free of charge from The Cambridge Crystallographic Data Centre via www.ccdc.cam.ac.uk/data_request/cif.

Table 3. Crystal data and refinement details for **1a** and **1b**.

	1a	**1b**
Empirical formula	$C_{70}H_{92}Cu_6N_8O_{14}$, 5 CH_2Cl_2	$C_{76}H_{104}Cu_6N_8O_{14}$, 6 THF
Formula weight	2075.39	2167.54
Crystal size [mm]	0.41 x 0.33 x 0.27	0.29 x 0.25 x 0.15
Cystal system	monoclinic	monoclinic
Space group	$P2_1/n$ (No. 14)	$P2_1/n$ (No. 14)
a [Å]	19.2213(6)	15.6652(8)
b [Å]	11.8722(4)	18.7972(8)
c [Å]	20.2856(6)	17.8818(8)
β [°]	100.605(2)	101.325(4)

V [Å^3]	4550.1(3)	5163.0(4)
$\rho_{calcd.}$ [g cm^{-3}]	1.515	1.394
Z	2	2
F(000)	2128	2284
μ (Mo-K$_\alpha$) [mm^{-1}]	1.732	1.283
T_{max}/T_{min}	0.7381 / 0.5193	0.8220 / 0.6680
hkl range	±22, ±13, ±23	±18, ±22, –21 to 20
θ range [°]	1.62 – 24.83	1.58 – 24.69
Measured refl.	70475	72143
Unique refl. [R_{int}]	7819 [0.0520]	8753 [0.1038]
Obs. refl. (I>2σ(I))	6183	5915
Refined parameters	534	604
Goodness-of-fit	1.027	0.999
R1 / wR2 (I>2σ(I))	0.0328 / 0.0779	0.0546 / 0.1236
R1 / wR2 (all data)	0.0455 / 0.0807	0.0922 / 0.1363
Resid. el. dens. [e Å^{-3}]	0.978 / –0.591	0.713 / –0.530

Supporting Information (see footnote on the first page of this article) Molecular structure of **1b**, UV/Vis spectrum for **1b**, ESI-MS spectrum for **1a**, EPR spectra for **1a** and table of all excitation energies ΔE.

Acknowledgment. Financial support by the Deutsche Forschungsgemeinschaft is gratefully acknowledged: SFB 602 (TP A16) and Heisenberg fellowship to A.H. (Project HO 2325/4-1).

References

1 (a) A. L. Gavrilova, B. Bosnich, *Chem. Rev*. **2004**, *104*, 349-384; (b) J. Klingele, S. Dechert, F. Meyer, *Coord. Chem. Rev.*, submitted.

2 (a) T. G. Schenck, J. M. Downes, C. R. C. Milne, P. Mackenzie, H. Boucher, J. Whelan, B. Bosnich, *Inorg. Chem.* **1985**, *24*, 2334-2337; (b) T. Kamiusuki, H. Okawa, E. Kitaura, M. Koikawa, N. Matsumoto, S. Kida, *J. Chem. Soc., Dalton Trans.* **1989**, 2077-2081; (c) M. Itoh, K.-i. Motoda, K. Shindo, T. Kamiusuki, H. Sakiyama, N. Matsumoto, H. Okawa, *J. Chem. Soc., Dalton Trans.* **1995**, 3635-3641; (d) F. Meyer, S. Beyreuther, K. Heinze, L. Zsolnai, *Chem. Ber./Recl.* **1997**, *130*, 605-613; (e) F. Meyer, K. Heinze, B. Nuber, L. Zsolnai, *J. Chem. Soc., Dalton Trans.* **1998**, 207-214; (f) M. Konrad, F.

Meyer, K. Heinze, L. Zsolnai, *J. Chem. Soc., Dalton Trans.* **1998**, 199-206; (g) L. Siegfried, T. A. Kaden, F. Meyer, P. Kircher, H. Pritzkow, *J. Chem. Soc., Dalton Trans.* **2001**, 2310-2315; (h) M. Konrad, S. Wuthe, F. Meyer, E. Kaifer, *Eur. J. Inorg. Chem.* **2001**, 2233-2240; (i) J. Ackermann, F. Meyer, H. Pritzkow, *Inorg. Chim. Acta* **2004**, *357*, 3703-3711; (j) J. C. Röder, F. Meyer, E. Kaifer, H. Pritzkow, *Eur. J. Inorg. Chem.* **2004**, 1646-1660; (k) A. Eisenwiener, M. Neuburger, T. A. Kaden, *Dalton Trans.* **2007**, 218-233; (l) D. J. de Geest, A. Noble, B. Moubaraki, K. S. Murray, D. S. Larsen, S. Brooker, *Dalton Trans.* **2007**, 467-475.

3 (a) J. C. Röder, F. Meyer, E. Kaifer, *Angew. Chem.* **2002**, *114*, 2414-2417; *Angew. Chem. Int. Ed.* **2002**, *41*, 2304-2306; (b) J. C. Röder, F. Meyer, R. F. Winter, I. Hyla-Kryspin, E. Kaifer, *Chem. Eur. J.* **2003**, *9*, 2636-2648; (c) T. Sheng, S. Dechert, I. Hyla-Kryspin, R. F. Winter, F. Meyer, *Inorg. Chem.* **2005**, *44*, 3863-3874.

4 (a) S. Demeshko, G. Leibeling, W. Maringgele, F. Meyer, C. Mennerich, H.-H. Klauss, H. Pritzkow, *Inorg. Chem.* **2005**, *44*, 519-528; (b) F. Meyer, S. Demeshko, G. Leibeling, E. Kaifer, H. Pritzkow*, Chem. – Eur. J.* **2005**, *11*, 1518-1526; (c) G. Leibeling, S. Demeshko, S. Dechert, F. Meyer, *Angew. Chem.* **2005**, *117*, 7273-7276; *Angew. Chem. Int. Ed.* **2005**, *44*, 7111-7114; (d) S. Demeshko, G. Leibeling, S. Dechert, F. Meyer, *Dalton Trans.* **2006**, 3458-3465; (e) C. Golze, A. Alfonsov, R. Klingeler, B. Büchner, V. Kataev, C. Mennerich, H.-H. Klauss, M. Goiran, J.-M. Broto, H. Rakoto, S. Demeshko, G. Leibeling, F. Meyer, *Phys. Rev. B.* **2006**, *73*, 224403; (f) S. Demeshko, G. Leibeling, S. Dechert, S. Fuchs, T. Pruschke, F. Meyer, *Chem. Phys. Chem.* **2007**, *8*, 405-417.

5 (a) F. Meyer, E. Kaifer, P. Kircher, K. Heinze, H. Pritzkow, *Chem. Eur. J.* **1999**, *5*, 1617-1630; (b) S. Buchler, F. Meyer, E. Kaifer, H. Pritzkow, *Inorg. Chim. Acta* **2002**, *337*, 371-386. (c) J. Ackermann, F. Meyer, E. Kaifer, H. Pritzkow, *Chem. Eur. J.* **2002**, *8*, 247-258; (d) B. Bauer-Siebenlist, F. Meyer, E. Farkas, D. Vidovic, J. A. C. Seijo, R. Herbst-Irmer, H. Pritzkow, *Inorg. Chem.* **2004**, *43*, 4189-4202; (e) B. Bauer-Siebenlist, F. Meyer, E. Farkas, D. Vidovic, S. Dechert, *Chem. Eur. J.* **2005**, *11*, 4349-4360; (f) B. Bauer-Siebenlist, S. Dechert, F. Meyer, *Chem. Eur. J.* **2005**, *11*, 5343-5352; (g) F. Meyer, *Eur. J. Inorg. Chem.* **2006**, 3789-3800; (h) J. Ackermann, S. Buchler, F. Meyer, *C.R. Chimie* **2007**, *10*, 421-432.

6 (a) T. G. Schenck, C. R. C. Milne, J. F. Sawyer, B. Bosnich, *Inorg. Chem.* **1985**, *24*, 2338-2344; (b) C. Dubs, A. Inagaki, M. Akita, *Chem. Commun.* **2004**, 2760-2761; (c) S. Tanaka, C. Dubs, A. Inagaki, M. Akita, *Organometallics* **2004**, *23*, 317-319; (d) C. Dubs, T. Yamamoto, A. Inagaki, M. Akita, *Organometallics* **2006**, *25*, 1359-1367; (e) U. J. Scheele, M. John, S. Dechert, F. Meyer, *Eur. J. Inorg. Chem.* **2008**, 373-377.

7 J. C. Röder, F. Meyer, H. Pritzkow, *Chem. Commun.* **2001**, 2176-2177.

8 G. Noël, J. C. Röder, S. Dechert, H. Pritzkow, L. Bolk, S. Mecking, F. Meyer, *Adv. Synth. Catal.* **2006**, *348*, 887-897.

9 G. Noël, A. Sachse, S. Dechert, F. Meyer, unpublished results.

10 J. C. Röder, F. Meyer, M. Konrad, S. Sandhöfner, E. Kaifer, H. Pritzkow, *Eur. J. Org. Chem.* **2001**, 4479-4487.

11 S. Teipel, K. Griesar, W. Haase, B. Krebs, *Inorg. Chem.* **1994**, *33*, 456-464.

12 L. Chen, S. R. Breeze, R. J. Rousseau, S. Wang, L. K. Thompson, *Inorg. Chem.* **1995**, *34*, 454-465.

13 S. Mukherjee, T. Weyhermüller, E. Bothe, K. Wieghardt, P. Chaudhuri, *Eur. J. Inorg. Chem.* **2003**, 863-875.

14 M. Bera, W. T. Wong, G. Aromi, J. Ribas, D. Ray, *Inorg. Chem.* **2004**, *43*, 4787-4789.

15 A. J. Blake, C. M. Grant, C. I. Gregory, S. Parsons, J. M. Rawson, D. Reed, R. E. P. Winpenny, *J. Chem. Soc., Dalton Trans.* **1995**, 163-175.

16 A. Bencini and D. Gatteschi, *EPR of Exchange Coupled Systems*. Springer, **1990**.

17 J. R. Pilbrow, *Transition Ion Electron Paramagnetic Resonance*, Clarendon Press, Oxford, **1990**.

18 W. L. Driessen, L. Chang, C. Finazzo, S. Gorter, D. Rehorst, J. Reedijk, M. Lutz, A. L. Spek, *Inorg. Chim. Acta* **2003**, *350*, 25-31.

19 O. Kahn, *Molecular Magnetism*, VCH Publishers Inc., New York, **1993**.

20 V. H. Crawford, H. W. Richardson, J. R. Wasson, D. J. Hodgson, W. E. Hatfield, *Inorg. Chem.* **1976**, *15*, 2107-2110.

21 P. E. Kruger, G. D. Fallon, B. Moubaraki, K. J. Berry, K. S. Murray, *Inorg. Chem.* **1995**, *34*, 4808-4814.

22 G.M. Sheldrick, SHELXL-97, Program for Crystal Structure Refinement, Universität Göttingen, Germany, **1997**; G.M. Sheldrick, SHELXS-97, Program for Crystal Structure Solution, Universität Göttingen, Germany, **1997**.

23 STOE & CIE GmbH, X-RED, Darmstadt, Germany, **2002**.

SUPPORTING INFORMATION

Title: Bulky pyrazolate-based compartmental ligand scaffolds: encapsulation of an edge-sharing Cu_6O_2 bitetrahdral core

Author(s): Anna Sachse, Gilles Noël, Sebastian Dechert, Serhiy Demeshko, Andreas Honecker, Alexei Alfonsov, Vladislav Kataev and Franc Meyer*

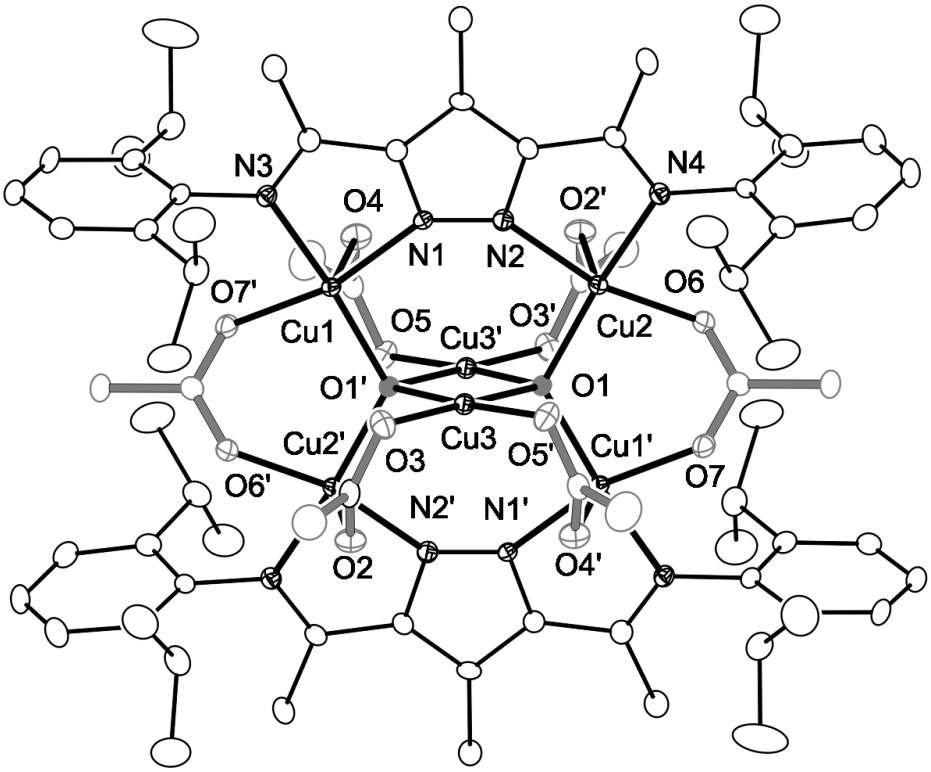

Figure S1. ORTEP plot (30% probability thermal ellipsoids) of the molecular structure of **1b**. For the sake of clarity all hydrogen atoms have been omitted. Symmetry transformation used to generate equivalent atoms: (') $-x+3, -y+2, -z$.

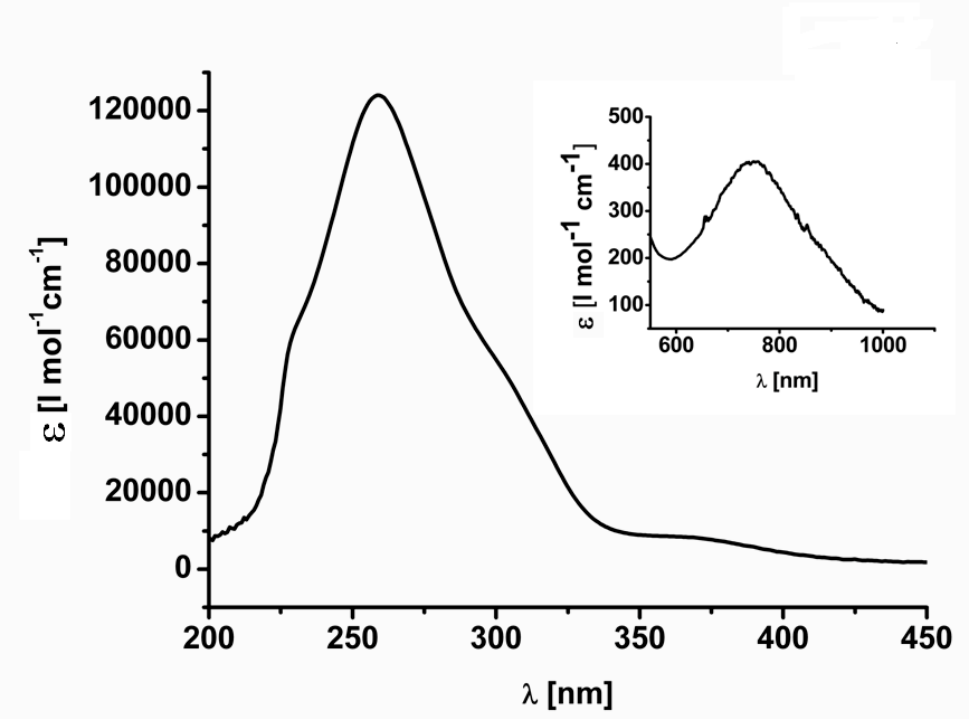

Figure S2. UV/Vis spectrum for **1b** in CH_2Cl_2 solution; The inset shows an enlargement of the d-d transition band for the Cu^{II} ions with λ_{max} = 748 nm (ε = 405 $l \cdot mol^{-1} \cdot cm^{-1}$).

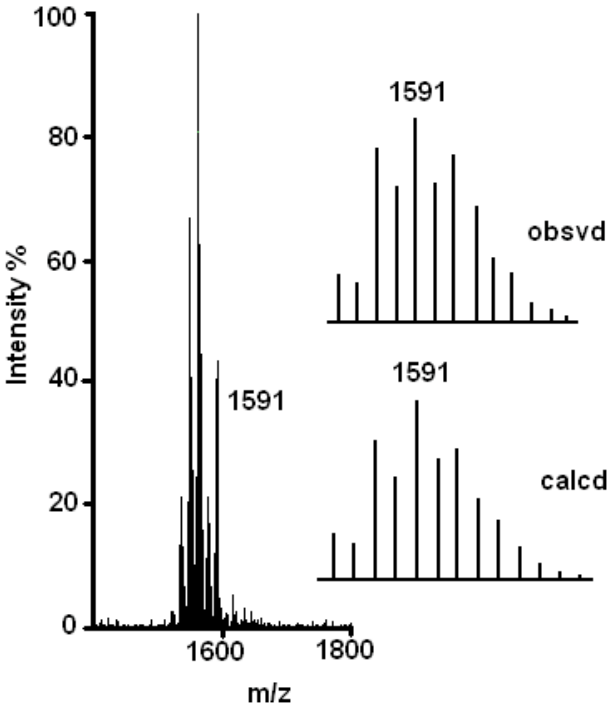

Figure S3. Positive ion ESI-MS spectrum for **1a** in MeCN / CH_2Cl_2 solution; the inset shows the experimental and calculated isotopic distribution for the peak at *m*/*z* 1591 corresponding to $[L^1{}_2Cu_6O_2(OAc)_5]^+$.

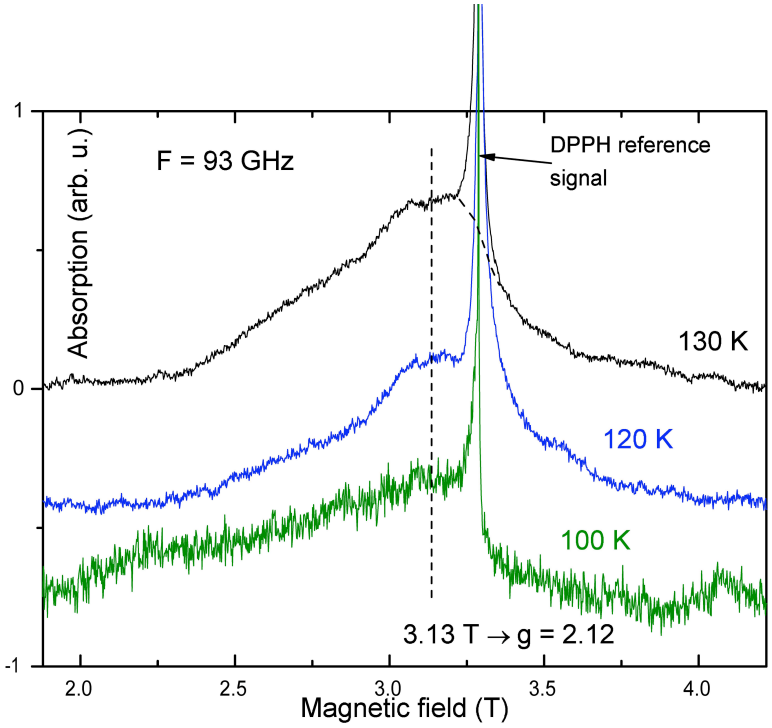

Figure S4. 93 GHz EPR spectra for **1a** at 100 K (green), 120 K (blue), and 130 K (black). The sharp resonance line is due to the DPPH field marker.

Table S1. All excitation energies ΔE classified by total spin S for four different sets (a) – (d) of exchange constants, in Kelvin and cm^{-1} (in brackets).

(a)		(b)		(c)		(d)	
J_1 = - 68.5 (-47.6)		J_1 = -125.4 (-87.2)		J_1 = -164.8 (-114.5)		J_1 = -69.7 (-48.4)	
J_2 = -161.9 (-112.5)		J_2 = -100.8 (-70.1)		J_2 = -78.4 (-54.5)		J_2 = -135.7 (-94.3)	
J_3 = -59.7 (-41.5)		J_3 = 151.4 (105.2)		J_3 = -50.6 (-35.2)		J_3 = 59.0 (41.0)	
$J_5 = J_4$ = 52.9 (36.7)		$J_5 = J_4$ = -6.2 (-4.3)		$J_5 = J_4$ = 39.1 (27.2)		$J_5 = J_4$ = 12.5 (8.7)	
S	ΔE	S	ΔE	S	ΔE	S	ΔE
0	0	0	0	0	0	0	0
1	136.9	1	137.0	1	137.7	1	139.3
1	283.7	1	250.8	1	238.9	1	227.9
2	314.9	2	338.6	0	275.3	2	342.3
1	403.1	0	362.9	1	294.5	1	345.8
2	434.3	1	375.4	1	329.6	1	392.2
1	526.3	2	400.3	2	389.0	0	417.1
0	567.3	1	439.7	2	395.6	2	460.2
1	607.5	1	552.0	2	490.2	2	499.3
0	632.1	2	577.0	1	545.5	1	510.1
2	638.7	3	614.4	2	545.8	0	535.0
1	645.7	1	641.4	3	568.7	3	588.8
3	652.4	0	665.7	1	604.9	1	617.3
1	704.3	1	678.1	0	623.7	2	663.6
2	726.9	2	703.1	1	646.7	0	691.7
0	751.5	0	867.3	1	702.3	1	713.5
1	850.2	0	879.5	0	724.9	2	731.7
0	955.9	1	879.8	0	780.5	1	781.5
2	969.6	2	904.7	2	803.4	0	806.5
1	1181.0	1	1130.3	1	959.9	1	831.0